
Capítulo 5

Trabajos Publicados

En esta sección se recogen los trabajos publicados durante la elaboración de esta tesis doctoral. Las publicaciones se presentan siguiendo el orden en que han ido apareciendo en el Capítulo Cuatro.

5.1 Publicación 1

TiO₂- photocatalyzed degradation of phenol and *ortho*-substituted phenolic compounds

Ana M. Peiró, José Antonio Ayllón, José Peral, Xavier Doménech
Departament de Química, Universitat Autònoma de Barcelona, 08193 Bellaterra,
Barcelona, Spain

Applied Catalysis B: Environmental 30 (2001) 359-373



TiO₂-photocatalyzed degradation of phenol and *ortho*-substituted phenolic compounds

Ana M. Peiró, José Antonio Ayllón, José Peral, Xavier Doménech*

Departament de Química, Universitat de Barcelona, 08193 Bellaterra, Barcelona, Spain

Received 21 May 2000; received in revised form 8 October 2000; accepted 8 October 2000

Abstract

The photocatalytic degradation of phenol, guaiacol, 2-chlorophenol and catechol in aqueous suspensions of TiO₂ under different experimental conditions has been investigated. The photodegradation of the different organics follows a Langmuir–Hinshelwood kinetics, showing rate constants that decrease in the order: guaiacol > 2-chlorophenol \cong phenol > catechol. A similar trend is also observed, except for catechol, for the stability of the σ -complexes that may be formed between the aromatic ring and the OH \bullet radical. From different analytical techniques (HPLC, GC/MS and HPLC/MS), various hydroxylated intermediate compounds have been reported and different mechanisms of degradation of the starting compounds have been proposed. From experiments performed using aqueous solutions containing the four organics, it is observed that the competitive Langmuir–Hinshelwood kinetics for the degradation of each one of the phenolic compounds is obeyed. © 2001 Elsevier Science B.V. All rights reserved.

Keywords: TiO₂; Photocatalysis; Phenols

1. Introduction

Photocatalysis is a subject of current interest in view of its application in effluent decontamination [1–3]. Particularly, photocatalysis takes advantage of its ability to generate hydroxyl radicals by oxidation of adsorbed OH[−] or H₂O molecules onto semiconductor surface upon irradiation with light of enough energy [3]. These OH \bullet radicals behave as powerful oxidants, which are able to degrade a great variety of organic compounds [4]. Phenols are, for different purposes, widely used chemicals and are present in a great variety of waste effluents of different industries, such as paper mills, chemical industries of production of

herbicides, fungicides, etc. [5]. These compounds are quite toxic and slowly degrade in the environment, giving different aromatic intermediates, most of them are also of environmental concern [6]. In this way, the use of photocatalysis has been proved to be a good choice to achieve a readily elimination of phenolic compounds [7].

In this paper, the kinetics and mechanisms of the photocatalytic degradation of phenol and three of its *ortho* derivatives, namely, guaiacol, 2-chlorophenol and catechol, which are toxic compounds commonly present in wastewaters produced by the pulp and paper industry, is investigated. The photocatalytic reactivity of these compounds is discussed in terms of the nature of the functional group of the different organics. Furthermore, the competitive effect between the phenolic compounds for photoreactive sites on the catalyst and

* Corresponding author.

E-mail address: xavier.domenech@uab.es (X. Doménech).

the kinetics of photocatalytic degradation of aqueous solutions containing the four organics is also studied.

2. Experimental

2.1. Reagents

All chemicals used were at least of reagent grade and were used as received. HPLC-grade eluents were employed. TiO₂ (Degussa P25) (80% anatase and 20% rutile and BET surface area: 59.1 m² g⁻¹). Solutions were prepared with water obtained from a Millipore Milli-Q system.

2.2. Photocatalytic experiments

Experiments were carried out in a thermostated cylindrical Pyrex cell of 100 cm³ of capacity. The reaction mixture inside the cell was maintained in suspension by magnetic stirring. In all experiments, air was bubbled continuously through the solution. As light source, a 125 W Philips HPK medium pressure mercury vapour lamp was used. The intensity of the incident light inside the photoreactor, measured employing an uranyl actinometer, was 2.3 × 10⁻⁵ einstein min⁻¹. The IR fraction of the incident beam was removed by the water in the double jacket of the photoreactor. All experiments were carried out at 25.0 ± 0.1 °C. The concentration of TiO₂ in suspension was 1.5 g dm⁻³. HClO₄ and NaOH were added in order to adjust the pH of the solutions. To remove particulates before analysis, the water samples were filtered through 0.45 μm pore size cellulose acetate filters.

2.3. Product analysis

Initial substrates degradation was followed by HPLC using a LC-10AD Shimadzu liquid chromatograph equipped with a 795A Applied Biosystems UV-VIS detector. The stationary phase was an Hiper-syl ODS column (25 cm, 4.6 mm (i.d.), 5 μm particles) working at room temperature. Experimental conditions for the liquid chromatography methods are shown in Table 1. Intermediate compounds formed during irradiation were determined by HPLC, GC/MS and HPLC/MS analysis. In GC/MS analysis, a 5890 Series II Hewlett Packard gas chromatograph provided with a TRB (1.30 m, 0.24 μm, 0.25 mm) column (apolar equivalent HP1) was employed. For detection, a quadrupole mass spectrometer (5989 A Hewlett Packard), provided with electronic impact was used. Spectra were recorded in the 40–400 uma range at 70 V. The GC was temperature programmed: the temperature of the injection and detector ports was held at 220 °C, and the GC oven temperature was maintained at 60 °C for 1 min and then it was increased to 280 °C at 5 °C/min. The final temperature was held for 5 min. Samples for GC/MS analysis were treated as follows: a 1 × 10⁻² mol dm⁻³ solution of the compound was irradiated for 19 h, after which intermediate products concentration was high enough to perform the analysis, and this irradiated solution was filtered by using a 0.45 μm pore size filter. Chloroform was used as extracting solvent, which was evaporated under N₂ flow after extraction. The coloured extracts were reconstituted with 100 μl of CHCl₃, and 1 μl sample of this extract was injected in the chromatograph, in split mode (1:60). In HPLC/MS analysis, a 1090 Hewlett Packard chromatograph provided with a diode array detector was employed. It was coupled

Table 1
Experimental conditions for the HPLC analysis

Analyte	Mobile phase composition	Flow rate (ml/min)	Wave length (nm)
Phenol	50% CH ₃ OH 50% H ₂ O	0.8	280
Catechol			
In kinetic studies	20% CH ₃ CN 80% H ₂ O pH = 3.0 H ₃ PO ₄	1.5	265
In studies of intermediate products	75% H ₂ O 20% CH ₃ OH 5% CH ₃ CN pH = 3.0 H ₃ PO ₄	0.7	265
2-Chlorophenol	10% CH ₃ CN 35% CH ₃ OH 55% H ₂ O	1.0	270
Guaiacol	40% CH ₃ OH 60% H ₂ O	0.8	270/280

to the previous mentioned mass spectrometer via a Particle Beam 59980 B Interface. A C18 (200, 21 cm) chromatographic column was used.

Total organic carbon (TOC) was determined with a Shimadzu TOC-5000 total organic carbon analyser.

Chloride ion determinations were carried out by ion chromatography using an IC Anion Column PRP-x100 (12.5 cm, 4.0 mm) and a conductimetric detector (Metrohm, mod.690). As a mobile phase, a 2 mmol dm^{-3} phthalic acid solution containing 10% acetone at pH 5.0 was employed at a flow rate of 1.00 ml min^{-1} .

In the study of guaiacol, an Aminex HPX 87C column at 35°C and 4 mmol dm^{-3} sulphuric acid solution were employed as stationary and mobile phase,

respectively to analyse short chain organic acids present in the solution.

3. Results and discussion

The time course of the concentration of different solutions of phenol, guaiacol, 2-chlorophenol and catechol has been studied under four different experimental conditions: (1) UV irradiation in absence of TiO_2 ; (2) at the dark in presence of TiO_2 ; (3) UV irradiation in presence of TiO_2 and (4) at the dark and in absence of TiO_2 . The concentration of the respective organic in each solution was $1000 \text{ } \mu\text{mol dm}^{-3}$ and the initial pH = 3.0. The obtained experimental results are depicted in Fig. 1. In all cases, the irradiation of TiO_2

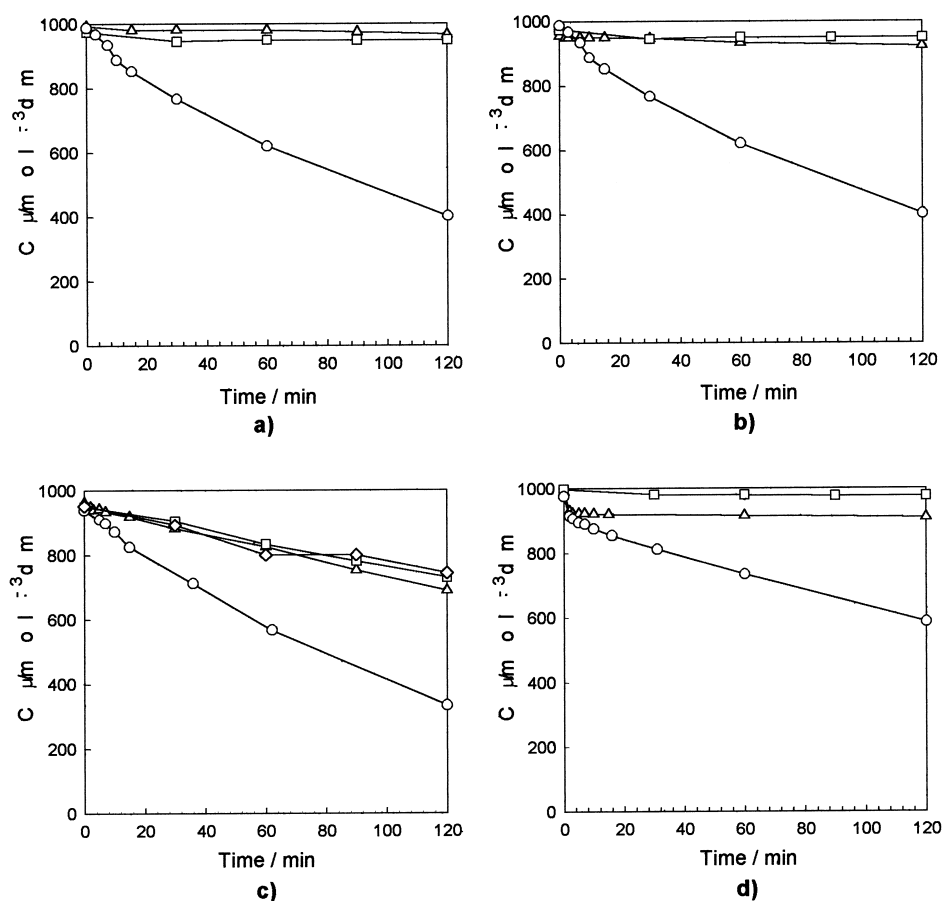


Fig. 1. Variation of the concentration of (a) phenol; (b) guaiacol; (c) 2-chlorophenol and (d) catechol, in aqueous solutions at pH = 3.0 under UV-illumination without TiO_2 (□), in the dark with TiO_2 (Δ), under UV-illumination with TiO_2 (o) and in the dark without TiO_2 (\diamond). Mass of TiO_2 in suspension: 1.5 g dm^{-3} , temperature: 25°C .

suspensions leads to the largest decrease of the organics concentration. Besides photocatalytic removal, for solutions of 2-chlorophenol a significant decrease of the organic compound, which is similar to the one obtained under the rest of the experimental conditions investigated, is noticed. In fact, this behavior is mainly due to air stripping of the organic compound, as it is observed after aerating a solution of $\mu\text{mol dm}^{-3}$ of 2-chlorophenol at $\text{pH} = 3.0$ in the dark and in absence of TiO_2 , for which a gradual decrease of organic is observed, being removed a 21.9% of its initial concentration after 2 h of aeration (see Fig. 1c). For the other organics, lower percentages removed by air stripping

were reported: 1.0, 3.7 and 0.8% for phenol, guaiacol and catechol, respectively, after 2 h of aeration.

On the other hand, the disappearance of the different organics by photocatalysis shows a low dependence on the pH of the suspensions in the pH range comprised between 3 and 10. However, with respect to TOC removal, the lowest yields are obtained in all cases for initial pH of 10 (see Fig. 2); the strongest dependence of TOC on pH is found for catechol solutions, for which a markedly decrease of the percentage of TOC removal with increasing pH is observed. At $\text{pH} = 10$, the surface charge of the semiconductor is predominantly negative (the pzc the TiO_2 used in this

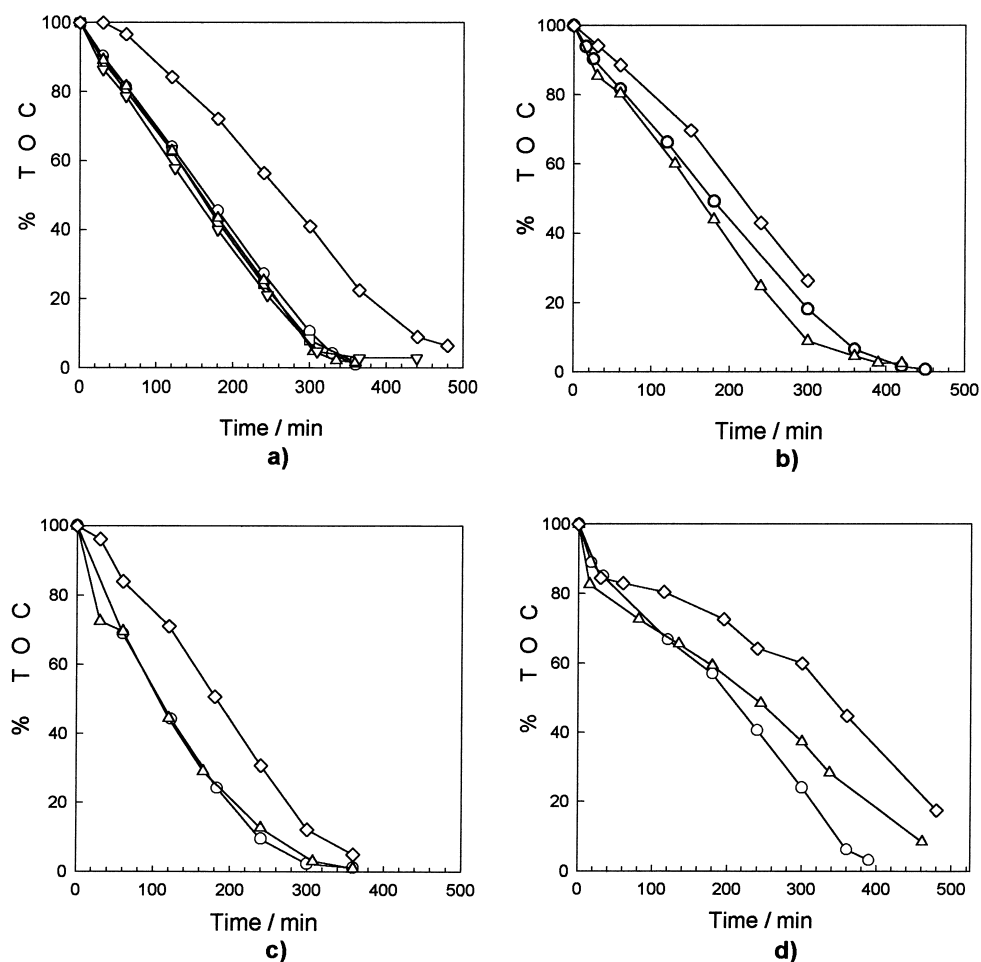


Fig. 2. Percentage of TOC removed time for aqueous suspensions under UV-illumination of (a) phenol; (b) guaiacol; (c) 2-chlorophenol and (d) catechol, at the following initial pHs 3.0 (o), 4.0 (\square), 6.0 (\triangle), 8.1 (∇) and 10.0 (\diamond) in presence of TiO_2 . Initial organic concentration: $1000 \mu\text{mol dm}^{-3}$, mass of TiO_2 in suspension: 1.5 g dm^{-3} , temperature: 25°C .

work is 6.25 [8]), hampering the adsorption of many of the hydroxylated aromatic intermediates formed during photocatalysis that, at this pH, probably exist as anionic species. In fact, HPLC analysis of the irradiated samples show the presence of more peaks in the chromatogram at pH 10 than at lower pHs at similar irradiation times, probably indicating a much lower ability of TiO_2 to adsorb the intermediates.

3.1. Kinetics of the photocatalytic process

Fig. 3 shows the time course of the photodegradation of the four organics for solutions of different initial concentrations ranging from 20 to 1000 $\mu\text{mol dm}^{-3}$ in presence of TiO_2 at $\text{pH} = 3.0$. From these

plots, the initial rates of photocatalytic degradation for the organic have been obtained. In Fig. 4, the plots $1/r_0$ versus $1/c_0$, where r_0 and c_0 are the initial rate of photodegradation and the initial concentration of organic, are represented for the four organics investigated. From these plots, and according to the Langmuir–Hinshelwood kinetics,

$$\frac{1}{r_0} = \frac{1}{k} + \left(\frac{1}{kK}\right) \frac{1}{c_0}$$

the values of the rate constant (k) and equilibrium adsorption constant (K) have been estimated; these values are summarised in Table 2.

The effect of substituents on the kinetics and reaction mechanisms of *para*-substituted phenols on

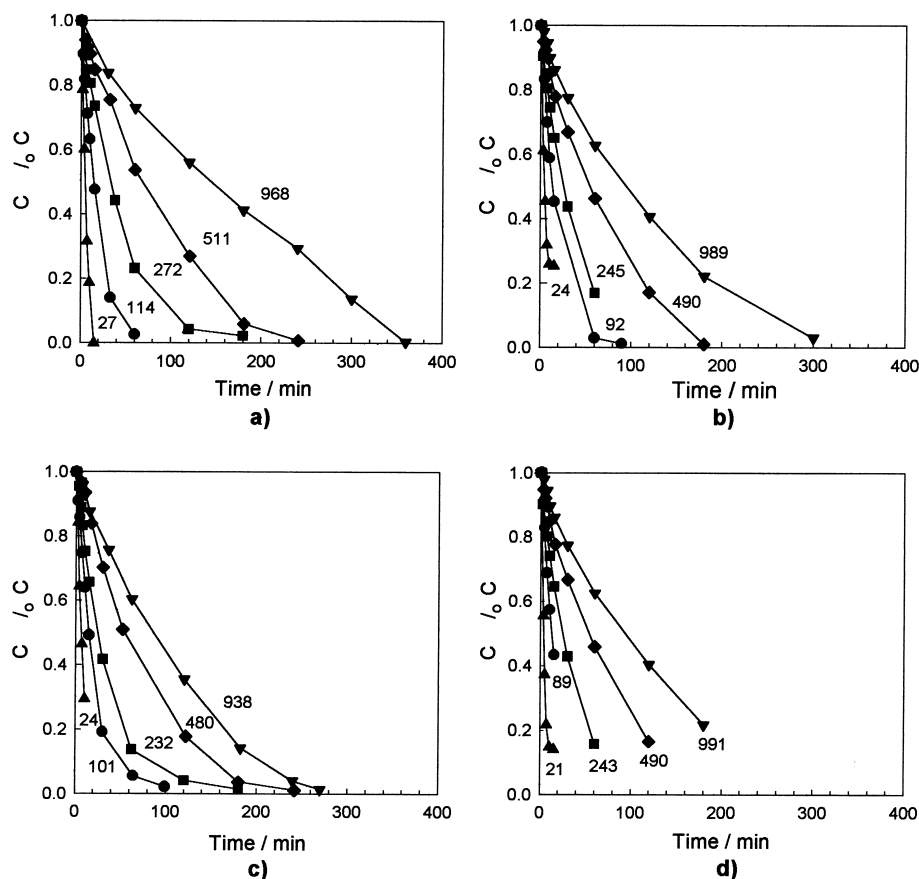


Fig. 3. Time course of (a) phenol; (b) guaiacol; (c) 2-chlorophenol and (d) catechol, for different initial concentrations of organics (in each curve, the initial concentration in $\mu\text{mol dm}^{-3}$ is given) under UV-illumination in presence of TiO_2 (1.5 g dm^{-3}) at initial $\text{pH} = 3.0$ and at 25°C .

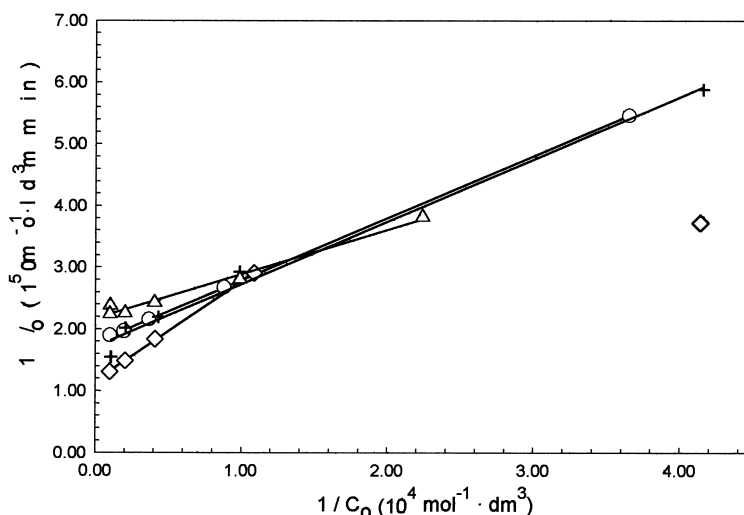


Fig. 4. Plot of the inverse of the initial rate of photocatalytic degradation respect to the inverse of the initial concentration for phenol (o), guaiacol (\diamond), 2-chlorophenol (+) and catechol (Δ). The experimental conditions are the same as reported in Fig. 3.

irradiated TiO_2 has been studied by O'Shea et al. in terms of Hammett correlations [9]. This treatment, however, usually fails with *ortho*-substituted compounds due to the *ortho*-effect [10], so a different approach is taken in the present work to inquire into the dependence of the degradation rate with the structure of the compounds under study.

In principle, it is expected that the extent of the photocatalytic degradation of the different organics depends on their reactivity towards the photogenerated OH^\bullet radical [11]. In fact, reactions between aromatic compounds and OH^\bullet radicals correspond to processes of hydrogen substitution, where the first step is the OH^\bullet complexation with the π -system of the aromatic ring, thus forming a π -complex in which the OH group has not a specific position in the molecule [7,12,13]. The second step corresponds to the formation of a σ -complex between the carbon atom of the ring, where

the substitution will take place, and the radical OH^\bullet [13].

The formation of the σ -complex is usually the rate determining step. With this assumption in mind, the energy of the reaction of the different organics with OH^\bullet radicals has been realized, by means of density functional theory (DFT) calculations by using the Gaussian 98 program. Both reaction energy calculations and geometry optimisation of organic compounds were performed by using Becke's hybrid B3LYP functional and the 6-31G + (d, p) basis set [14,15]. In all cases, it was assumed that the entry of the OH^\bullet radicals occurs in the *para* position respect to the $-\text{OH}$ group, since the latter is strongly *ortho-para* director in electrophilic aromatic substitutions; furthermore, the *para* position exhibits a lower steric hindrance than the *ortho* position [13]. From these estimates, the stability of the different σ -complexes

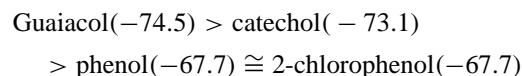
Table 2

Rate constants of photocatalytic degradation (k) and equilibrium adsorption constants (K) for phenol, guaiacol, 2-chlorophenol and catechol at 25°C^a

	Phenol	Guaiacol	2-Chlorophenol	Catechol
k ($\mu\text{mol dm}^{-3} \text{min}^{-1}$)	5.6 ± 0.1	8.6 ± 0.3	5.8 ± 0.4	4.6 ± 0.3
K ($10^4 \text{ dm}^{-3} \text{mol}^{-1}$)	1.77 ± 0.02	0.72 ± 0.03	1.7 ± 0.3	3.0 ± 0.5

^a Mass of TiO_2 in suspension = 1.5 g dm^{-3} and $\text{pH} = 3.0$.

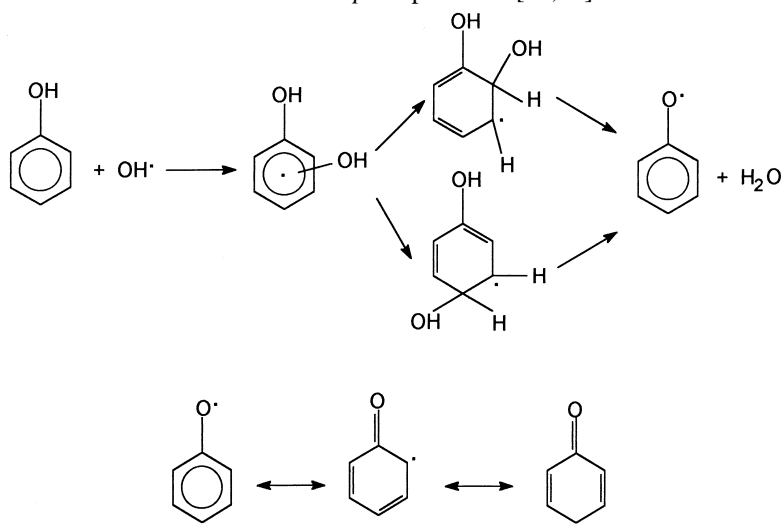
decreases in the order (in parenthesis, the energy of the reaction in kJ mol^{-1} is given),



which is similar to the observed trend of photocatalytic rate constants (see Table 2), except for catechol that has the lower k -value. Possibly, this model that describes the reactivity in homogeneous phase is not appropriate enough for catechol, which is the phenolic compound that shows the greater adsorption constant (Table 2). On the other hand, it must be pointed out that beside reaction with OH^\bullet radical, other processes such as direct reaction between organic substrate and photogenerated holes or O_2^\bullet radicals, although less relevant, can also proceed at the semiconductor–electrolyte interface [3].

by HPLC is shown. As can be seen, the maximum concentration of intermediates appears after 19 h of irradiation, just at 33% of the time required to fully degrade the phenol. A similar result is observed at the same experimental conditions but for an initial phenol concentration of $1000 \mu\text{mol dm}^{-3}$. At the irradiation time for which the intermediate maximum concentration is attained, a sample of the reactive mixture was withdrawn from the photoreactor and analyzed for intermediates afterwards, by using HPLC, HPLC/MS and GC/MS. Table 3 shows the intermediates detected by means of the different experimental techniques.

The intermediates detected can be rationalized assuming the existence of an activation of the phenol molecule by reaction with an OH^\bullet radical, forming an adduct that evolves to give a phenoxy radical; actually, this radical is in resonance with radical structures in *ortho* and *para* positions [12,16].



3.2. Intermediates and mechanism

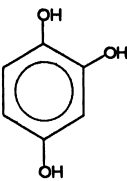
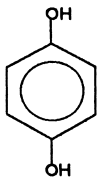
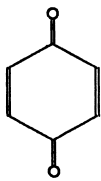
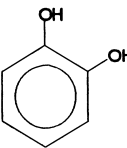
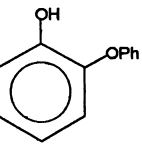
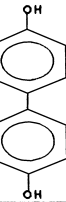
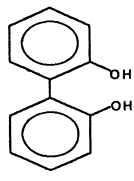
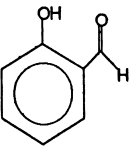
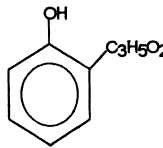
In this section, the mechanism of the photocatalytic degradation of phenol, guaiacol, 2-chlorophenol and catechol is described in terms of the main intermediates detected.

3.2.1. Phenol

In order to detect the aromatic intermediates formed during photocatalysis, a solution of 0.01 mol dm^{-3} of phenol at $\text{pH} = 3.0$ has been used. In Fig. 5 the time course of phenol and the main intermediates detected

These three mesomeric forms of the radical are the starting point of the formation of the different intermediates detected (see Scheme 1). Thus, these radicals can react with OH^\bullet to form more hydroxylated compounds such as catechol, hydroquinone or benzoquinone. On the other hand, the direct coupling of two phenoxy radicals can lead to the formation of the more complex intermediates molecules with two aromatic rings [17]. In the case of the hydroxybenzaldehyde intermediate, it is suggested that it can be formed by the direct attack of the radical CHO^\bullet to the *ortho* position of phenol; this radical, could be

Table 3
Intermediates detected by means of different analytical techniques after 19 h irradiation of an initial 0.01 mol dm^{-3} solution of phenol at initial pH of 3.0 in presence of TiO_2

									
HPLC	x	x	x	x					
HPLC/MS			x	x					
GC/MS		x	x		x	x	x	x	x

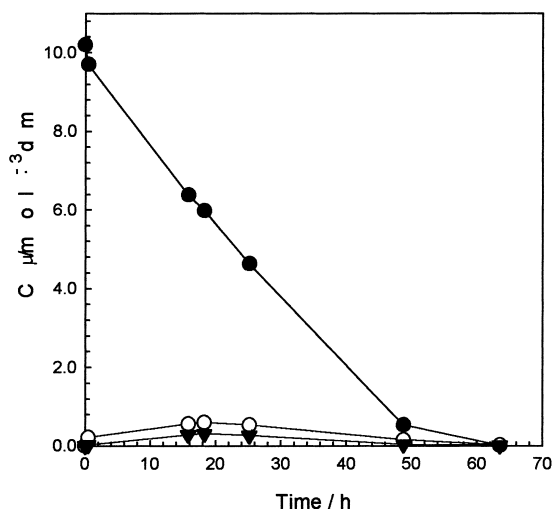
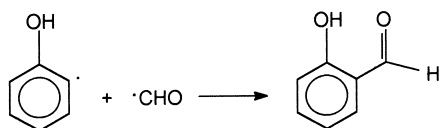


Fig. 5. Time course of the concentration of phenol (●) as well as the intermediate catechol (▽) and hydroquinone (○) formed during UV-illumination of initial 0.01 mol dm^{-3} aqueous solutions of phenol at $\text{pH} = 3.0$ in presence of TiO_2 (1.5 g dm^{-3}) at 25°C .

formed in intermediate steps of the oxidation process. In fact, the CHO^\bullet radical has been detected during the oxidation of formaldehyde by OH^\bullet radical and by photocatalysis over ZnO in aqueous solution [18–20].

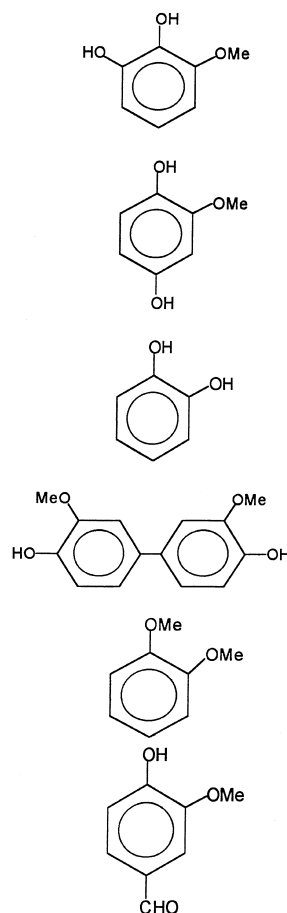


3.2.2. Guaiacol

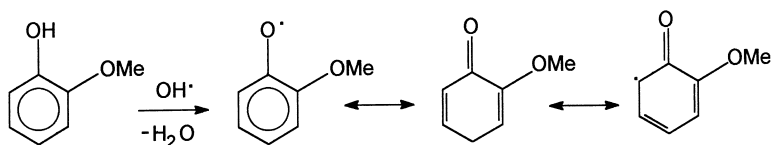
The main intermediates detected by GC/MS during photocatalytic degradation of guaiacol are listed in Table 4. Three intermediates were not unequivocally identified, which appeared at 10.825 min (MW = 138); 32.636 min (MW = 246) and 33.115 min (MW = 246). The former may correspond to a dimethoxybenzene isomer and the other ones to dimethoxydihydroxybiphenyl isomers; this suggestion

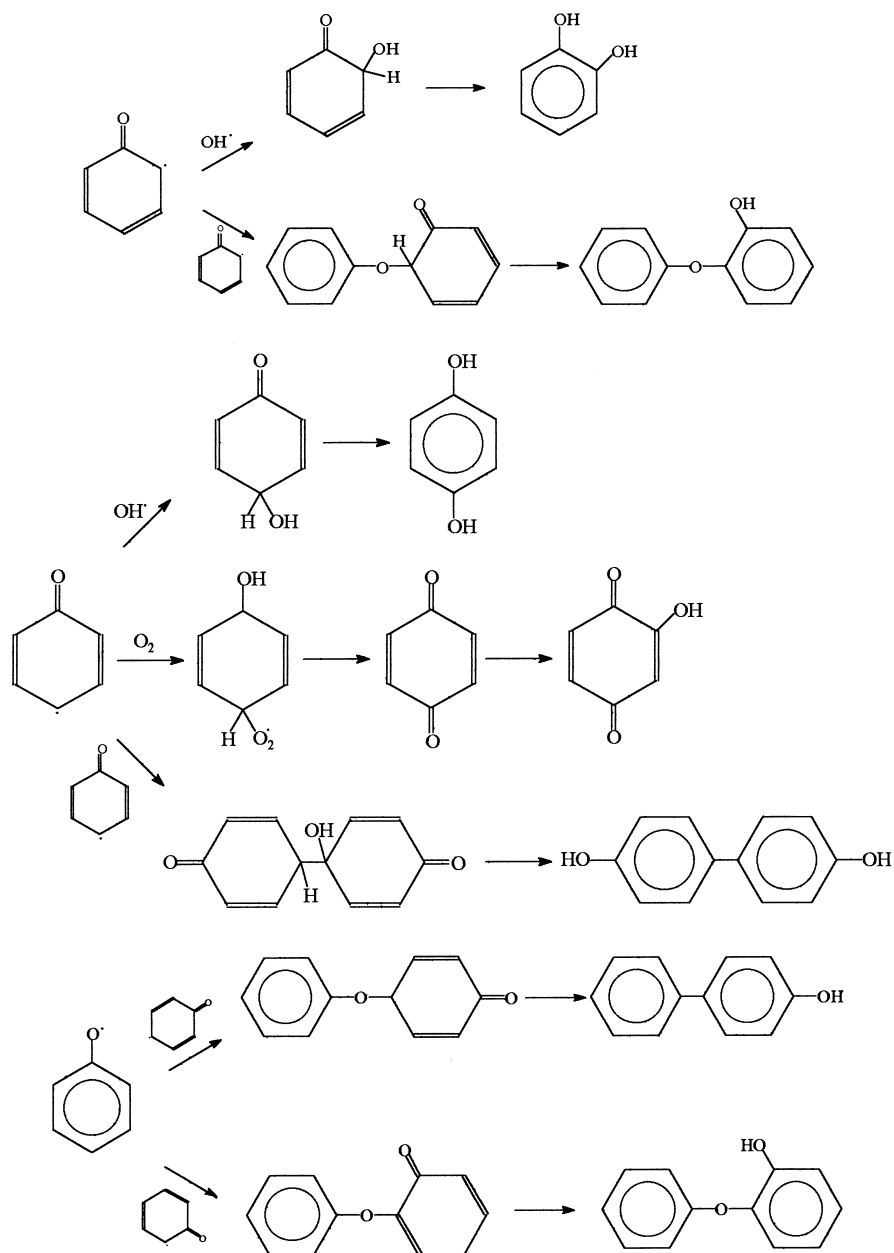
Table 4

Intermediates detected by means of GC/MS after 19 h irradiation of an initial 0.01 mol dm^{-3} solution of guaiacol at initial pH of 3.0 in presence of TiO_2



is based on the molecular weights of these compounds, their fragment peaks and the similarity of their retention times with those of the corresponding identified isomers. The sample used to perform this analysis was obtained after 20 h irradiation of 0.01 mol dm^{-3} of guaiacol in presence of TiO_2 at $\text{pH} = 3.0$. Similarly to phenol, the first step in the photodegradation of guaiacol, is the formation of a ring radical by reaction between guaiacol and OH^\bullet :

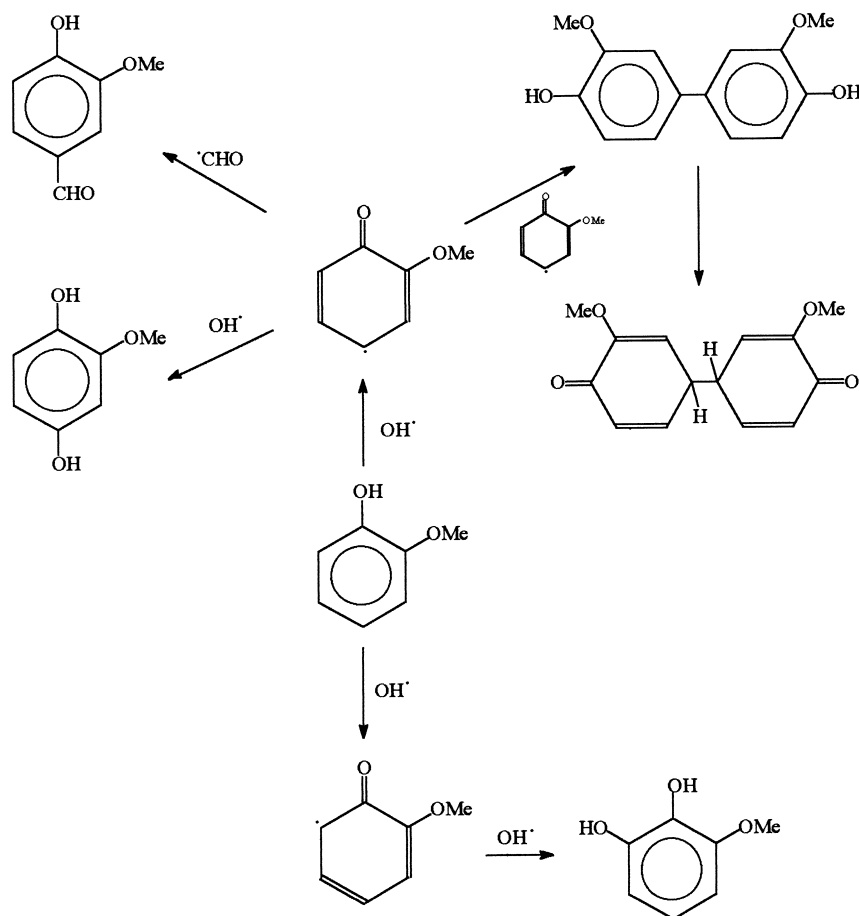




Scheme 1. Mechanism suggested for the intermediates detected in the photocatalytic degradation of phenol.

Scheme 2 shows the different reaction pathways for the formation of the detected intermediates, including the most complex biphenyl intermediate, 3,3'-dimethoxy-4,4'-dihydroxybiphenyl; in fact, the latter compound has also been detected during oxi-

dation of guaiacol by peroxidase enzymes in presence of H_2O_2 [21]. On the other hand, glycolic acid has been detected by means of ion exchange chromatography. This intermediate is believed to be formed in the last steps of the photodegradation process due to the



Scheme 2. Mechanism suggested for the intermediates detected in the photocatalytic degradation of guaiacol.

breaking of the aromatic ring. Neither fumaric, maleic nor oxalic acids were detected by this technique.

3.2.3. 2-Chlorophenol

During photocatalytic degradation of 2-chlorophenol, a gradual release of Cl^- ions into solution is observed. Fig. 6 shows the time course of 2-chlorophenol and Cl^- ion, in illuminated solutions of $930 \mu\text{mol dm}^{-3}$ of the former at $\text{pH} = 3.0$ in presence of TiO_2 at 25°C . As can be seen, the concentration of Cl^- ions attains a limiting value of $800 \mu\text{mol dm}^{-3}$ after about 5 h of irradiation, just when all chlorophenol has disappeared; this value of Cl^- concentration released to the solution corresponds to 86% of chlorine atoms initially present in the

2-chlorophenol molecules; probably, the remaining Cl is found in solution forming chloroderivative intermediates; some of these organochlorine intermediates have been detected by GC/MS analysis of a sample obtained by irradiating a solution of 0.01 mol dm^{-3} of 2-chlorophenol in presence of TiO_2 at $\text{pH} = 3.0$ (see Table 5). Scheme 3 illustrates the mechanism of formation of these intermediates. It has been suggested, that these intermediates are formed by hydroxylation of 2-chlorophenol in *para*, which is a high electron density position, to give 2-chloro, 1,4-dihydroxi benzene [22]. Another possibility is the substitution of Cl atom by an OH to give catechol [22]. On the other hand, 3-chlorophenol and 2,4-dichlorophenol can be produced by the addition of Cl^\bullet radicals to phenol and

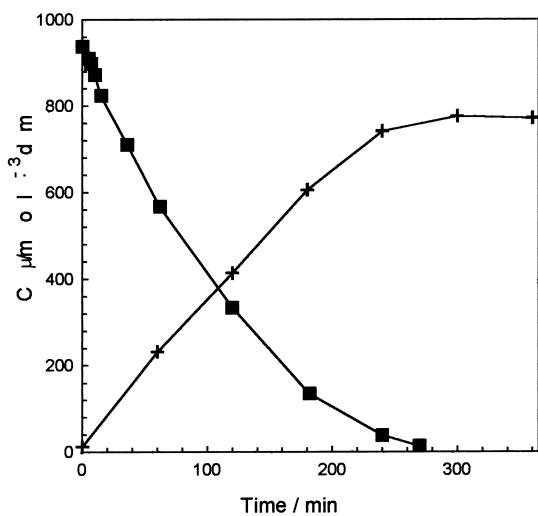
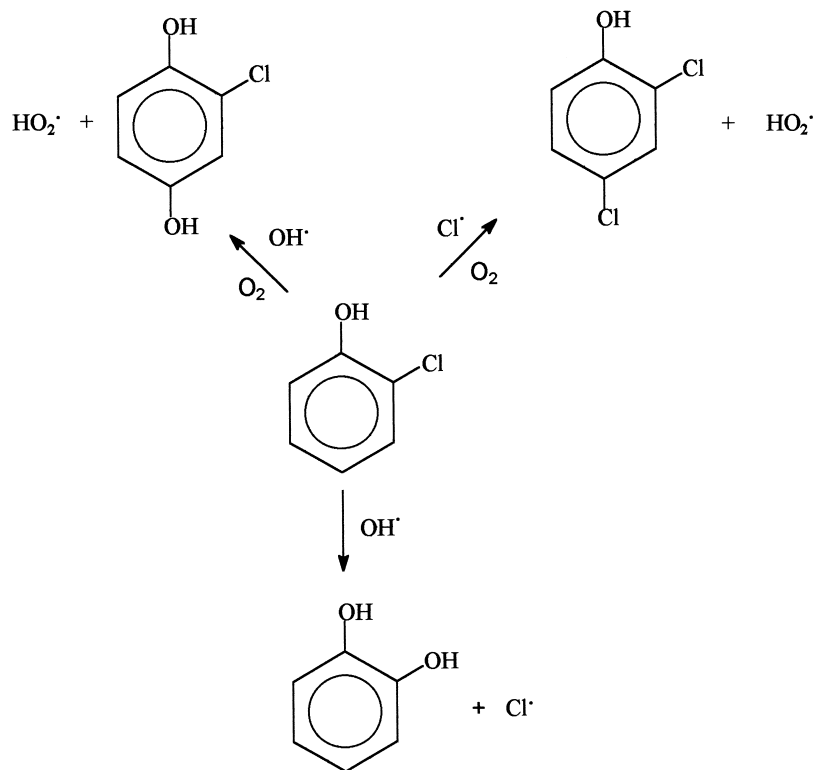
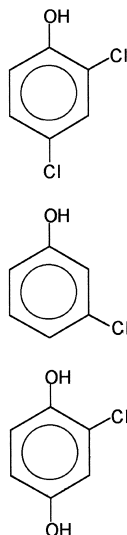


Fig. 6. Time course of the concentrations of 2-chlorophenol (\square) and chloride ions (+) released due to photodegradation of the former in presence of TiO_2 (1.5 g dm^{-3}) at initial pH of 3.0 and at 25°C .

Table 5
Intermediates detected by means of GC/MS after 19 h irradiation of an initial 0.01 mol dm^{-3} solution of 2-chlorophenol at initial pH of 3.0 in presence of TiO_2



Scheme 3. Mechanism suggested for the intermediates detected in the photocatalytic degradation of 2-chlorophenol.

2-chlorophenol, respectively; Cl^\bullet radicals can be formed by direct photolysis of 2-chlorophenol and of other chlororganics present in the solution mixture [23].

3.2.4. Catechol

The photocatalytic degradation of catechol gives highly polar intermediates that are difficult to detect by the analytic techniques used in the present work; some of the peaks detected by HPLC would be attributed to 1,2,3- and 1,2,4-benzenetriol, while signals ascribed to *para*-ethoxyphenol and *para*-phenoxyphenol have been obtained by GC/MS; although completely reliance on this assignment needs further evidence. It must be said that catechol and the highly polar intermediates formed during irradiation are strongly adsorbed onto TiO_2 particles, giving rise to their rapid degradation [24,25].

3.3. Kinetics of the multicomponent system

The photocatalytic degradation of a solution containing a mixture of the four organics has been studied. In Fig. 7, the time course of the percentage of TOC removal in a solution containing equimolar concentrations of phenol, guaiacol, 2-chlorophenol and catechol, up to a total concentration of $1000 \mu\text{mol dm}^{-3}$

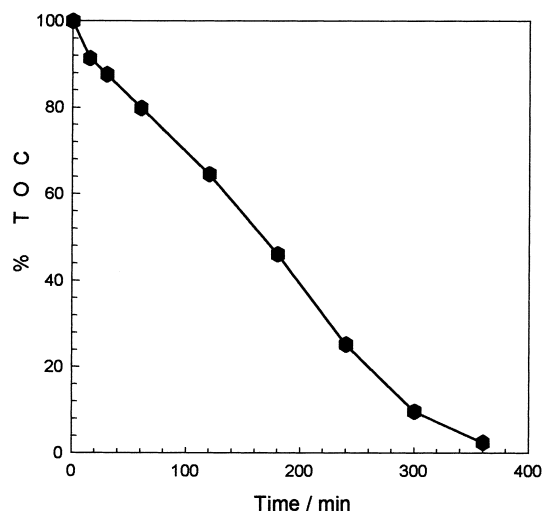


Fig. 7. Variation with time of the percentage of TOC for a solution of an equimolar mixture of phenol, guaiacol, 2-chlorophenol and catechol at an initial total concentration of $\mu\text{mol dm}^{-3}$ at initial pH of 3.0 under UV-illumination in presence of TiO_2 (1.5 g dm^{-3}) at 25°C .

at $\text{pH} = 3.0$ and in presence of TiO_2 is depicted. After 6 h of irradiation, 97.5% of TOC is being removed and the pH of the suspension decreases only 0.2 units. In Fig. 8, the variation of the concentration of the individual organics in the mixture as a function of the

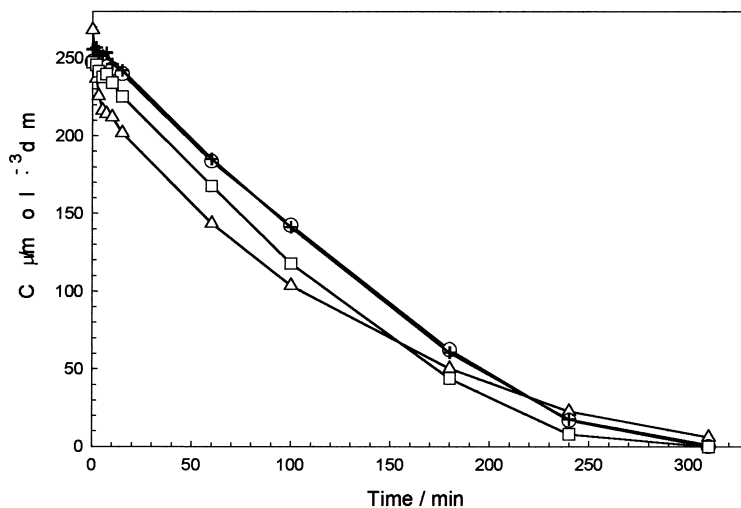


Fig. 8. Time course of the concentration ratio of the individual organics during UV-illumination of an aqueous mixture of equimolar phenol (o), guaiacol (+), 2-chlorophenol (□) and catechol (△). Experimental conditions: the same as detailed in Fig. 7.

Table 6

Experimental and estimated initial rates of photodegradation of phenol, guaiacol, 2-chlorophenol and catechol in photocatalyzed aqueous solutions of a mixture of these organics at an overall concentration of $1020 \mu\text{mol dm}^{-3}$ at initial pH of 3.0 and at 25°C

	Phenol	Guaiacol	2-Chlorophenol	Catechol
Initial concentration ($\mu\text{mol dm}^{-3}$)	248	256	247	268
Initial rate (exp.) ($\mu\text{mol}^{-1} \text{dm}^{-3} \text{min}^{-1}$)	0.5 ± 0.1	1.0 ± 0.2	1.4 ± 0.4	1.8 ± 0.8
Initial rate (calc.) ($\mu\text{mol}^{-1} \text{dm}^{-3} \text{min}^{-1}$)	1.3 ± 0.2	0.8 ± 0.2	1.3 ± 0.5	2.0 ± 0.7

irradiation time is represented. From these curves, the initial rates of photodegradation for each one of the organics is estimated and listed in Table 6, together with the initial rates of photocatalytic degradation calculated using the Langmuir–Hinshelwood model for competitive kinetics,

$$r_i = \frac{k_i K_i c_i}{1 + \sum K_i c_i}$$

where the kinetic rate constant (k_i), the equilibrium adsorption constant (K_i) and the concentration (c_i) for the different organics that compete for the reaction sites on the photocatalyst surface are considered. As it is shown in Table 6, the experimental and calculated initial rates of photodegradation of the four organics agree within the experimental error, except in the case of phenol that has an experimental value moderately lower than the estimated by the Langmuir–Hinshelwood model. However, owing to the experimental error limits in the measured initial rates it is difficult to obtain any quantitative assumptions.

4. Conclusions

The UV irradiation of aerated aqueous solutions of phenol, guaiacol, 2-chlorophenol and catechol containing TiO_2 in suspension leads to the total elimination of the organic content in solution, being this process less efficient for highly alkaline solutions. The photocatalytic degradation of the four organics studied obeys a Langmuir–Hinshelwood kinetics with rate constants decreasing in the order: guaiacol > 2-chlorophenol \cong phenol > catechol, that is the same as the order obtained for the stability of the σ -complexes estimated theoretically from homogeneous reaction between the aromatic rings and radical

OH^\bullet , except for catechol, probably due to its strong adsorption onto photocatalyst.

On the other hand, a diversity of highly hydroxylated intermediates have been detected after irradiating the corresponding phenolic solutions in the presence of TiO_2 . The formation of two-rings intermediates has been detected, that has been assumed to be formed by direct coupling of phenoxy radicals. Finally, it has been observed from studies performed with aqueous solutions containing a mixture of the four organics, that the simple Langmuir–Hinshelwood kinetics can be applied to account for the competition between the different organic molecules for the reactive sites onto the photocatalyst.

Acknowledgements

The authors wish to thank to Luís Rodríguez for his help in performing the theoretical estimates, and to CICYT (AMB99-1212-C03-01) for financial support.

References

- [1] D. Martínez Plaza, S. Malato, *Catálisis Today* 54 (1999) 191.
- [2] M. Litter, *Appl. Catal. B* 23 (1999) 89.
- [3] M.R. Hoffmann, S.T. Martin, W. Choi, D. Bahnemann, *Chem. Rev.* 95 (1995) 69.
- [4] W.H. Galze, *Environ. Sci. Technol.* 21 (1987) 224.
- [5] C. Baird, *Environmental Chemistry*, Freeman, New York, 1998, p. 330.
- [6] R.P. Schwarzenbach, P.M. Gschwend, D.M. Imboden, *Environmental Organic Chemistry*, Wiley, New York, 1993, p. 501.
- [7] V. Brezová, S. Stasko, *J. Catal.* 147 (1994) 156.
- [8] M. Trillas, J. Peral, X. Domènech, *Appl. Catal. B* 5 (1995) 337.
- [9] K.E. O'Shea, C. Cardona, *J. Org. Chem.* 59 (1994) 5005.
- [10] L.P. Hammett, *Physical Organic Chemistry*, McGraw-Hill, New York, 1940, p. 204.

- [11] G. Marci, A. Scalfani, V. Augugliaro, L. Palmisano, M. Schiavello, *J. Photochem. Photobiol. A: Chem.* 9 (1995) 69.
- [12] R. Niessen, C. Lenoir, P. Boule, *Chemosphere* 17 (1988) 1977.
- [13] F.A. Carey, R.J. Sundberg, *Advanced Organic Chemistry. Part A. Structure and Mechanisms*, 3rd Edition, Plenum Press, New York, 1990.
- [14] A.D. Becke, *J. Chem. Phys.* 98 (1993), pages 1372, 5648.
- [15] P.J. Stephens, F.J. Devlin, C.F. Chablowski, M.J. Frisch, *J. Phys. Chem.* 98 (1994) 11623.
- [16] K. Okamoto, Y. Yamamoto, H. Tanaka, M. Tanmaka, A. Itaya, *Bull. Chem. Soc. Jpn.* 58 (1985) 2023.
- [17] D.A. Whiting, Oxidative coupling of phenols and phenols ethers, in: Barry M. Trost (Ed.), *Comprehensive Organic Synthesis: Selectivity, Strategy and Efficiency in Modern Organic Chemistry. Carbon–Carbon σ -Bond Formation*, Vol. 3, Pergamon Press, New York, 1991.
- [18] C. Lamy, B. Beden, J.M. Leger, *Electrochim. Acta* 35 (1990) 679.
- [19] W.J. McElroy, S.J. Waygood, *J. Chem. Soc., Faraday Trans. 87* (1991) 1513.
- [20] Z. Yiheng, C. Qi, Z. Yu, Y. Tiantang, Y. Shuqin, Z. Siyong, *Huaxue Wuli Xuebao* 11 (1998) 461.
- [21] D.R. Doerge, R.L. Divi, M.J. Churchwell, *Anal. Biochem.* 250 (1997) 10.
- [22] N. Gettof, *Solar, Radiat. Phys. Chem.* 28 (1986) 443.
- [23] M. Barbeni, E. Premauro, E. Pellizzetti, M. Grätzel, N. Serpone, *N.J. Chem.* 8 (1984) 550.
- [24] D.F. Ollis, E. Pelizzetti, N. Serpone, *Heterogeneous photocatalysis in the environment: application to water purification*, in: N. Serpone, E. Pellizzetti (Eds.), *Photocatalysis Fundamentals and Application*, Wiley, New York, 1989, p. 609.
- [25] S. Dagley, P.J. Chapman, D.T. Gibson, J.M. Wood, *Nature* 202 (1964) 775.

5.2 Publicación 2

Low- Temperature Deposition of TiO₂ Thin Films with Photocatalytic Activity from Colloidal Anatase Aqueous Solutions

Ana M. Peiró,^a José Peral,^a Concepción Domingo,^b Xavier Domènech^a and José A. Ayllón^a

^a Departament de Química, Universitat Autònoma de Barcelona,
08193 Bellaterra, Barcelona, Spain

^b Institut de Ciència de Materials de Barcelona (CSIC) Campus de la UAB,
08193 Bellaterra, Barcelona, Spain

Chemistry of Materials 13 (8) (2001) 2567-2573

Low-Temperature Deposition of TiO₂ Thin Films with Photocatalytic Activity from Colloidal Anatase Aqueous Solutions

Ana M. Peiró,[†] José Peral,[†] Concepción Domingo,[‡] Xavier Domènech,[†] and José A. Ayllón^{*,†}

Departament de Química, Universitat Autònoma de Barcelona, 08193 Bellaterra, Spain, and Institut de Ciència de Materials de Barcelona, CSIC, 08193 Bellaterra, Spain

Received December 4, 2000

Crystalline TiO₂ films have been deposited on several substrates (glass, F-doped SnO₂-covered glass, and silicon wafers) by a drain-coating method from a colloidal anatase aqueous solution. The process is performed at low-temperature, 333 K, in open atmosphere. The colloidal TiO₂ consists on anatase nanoparticles of about 9 × 5 nm size, stabilized by tetrabutylammonium cations (TBA⁺). This colloid has also been obtained under mild conditions (i.e., low temperature and ambient pressure) by hydrolysis of tetrakispropyl orthotitanate (TIP) in the presence of (TBA)OH and subsequent treatment by microwave radiation to enhance crystallization. Different film thicknesses have been obtained by consecutive deposition processes. Titania films thus obtained were transparent and showed good adherence. FT-IR analysis of the films reveal that TBA cations were not trapped in the film during the deposition process. No further thermal posttreatment was required to eliminate organics from the films or to induce titania crystallization. The photocatalytic activity of as-deposited titania has been assessed by the photodegradation of salicylic acid in aqueous solution under aerated conditions.

Introduction

Titanium dioxide has found extensive use in a great variety of applications. TiO₂ coatings are used in dye-sensitized photoelectrochemical cells,¹ as antireflection material in solar cells,² as gas sensors,³ in photoelectrocatalysis,⁴ and in photocatalysis.⁵ In this latter case, the possibility of having the material supported on an inert substrate is especially interesting for wastewater and indoor atmospheres remediation⁶ since problems derived from photocatalyst filtering are avoided. A variety of physical and chemical approaches have been used for TiO₂ thin-film preparation. Physical methods

include sputtering,⁷ CVD,⁸ MOCVD,⁹ light-induced CVD,¹⁰ pulsed laser deposition,¹¹ ion-assisted electron-beam evaporation,¹² atomic layer deposition,¹³ etc. These methods require a high amount of energy that is reemitted in part as exhaust heat or in the exhaust gases. Recently, efforts have been made to produce these films through chemical routes (wet methods), which are less energy consuming and do not require vacuum equipment. They include, among other, sol-gel methods,¹⁴ electrochemical deposition,¹⁵ Langmuir-Blodgett films,¹⁶ and crystallization on functionalized surfaces.¹⁷ A relatively simple and inexpensive chemical approach involves casting of thin films directly from colloidal semiconductor suspensions,¹⁸ the main interest of these

* To whom all correspondence should be addressed. Telephone: (+34) 93 581 29 19. Fax: (+34) 93 581 29 20. E-mail: joseantonio.ayllon@uab.es.

[†] Universitat Autònoma de Barcelona.

[‡] Institut de Ciència de Materials de Barcelona.

(1) (a) Thompson, D. W.; Kelli, C. A.; Farzad, F.; Meyer, G. *Langmuir* **1999**, *15*, 650. (b) Tennakone, K.; Senadeera, G. K. R.; Perera, V. P. S.; Kottegoda, I. R. M.; de Silva, L. A. A. *Chem. Mater.* **1999**, *11*, 2474. (c) Li, Y.; Hagen, J.; Schaffrath, W.; Otschik, P.; Haarer, D. *Sol. Energy Mater. Sol. Cells* **1999**, *56*, 167.

(2) (a) Gee, J. M.; Gordon, R.; Liang, H. <http://www.sandia.gov/pv/comp/cells1.htm>. (b) Doeswijk, L. M.; de Moor, H. H. C.; Blank, D. H. A.; Rogalla, H. *Appl. Phys. A* **1999**, *69*, S409.

(3) Lin, H. M.; Keng, C. H.; Tung, C. Y. *Nanostruct. Mater.* **1997**, *9*, 747.

(4) (a) Rodríguez, J.; Gómez, M.; Lindquist, S.-E.; Granquist, C. G. *Thin Solid Films* **2000**, *360*, 250. (b) Gerischer, H. *Electrochim. Acta* **1993**, *38*, 3. (c) Ichikawa, S.; Doi, R. *Thin Solid Films* **1997**, *292*, 130.

(5) Xagas, A. P.; Androulak, E.; Hiskia, A.; Falaras, P. *Thin Solid Films* **1999**, *357*, 173.

(6) (a) Byrne, J. A.; Eggins, B. R.; Brown, N. M. D.; McKinney, B.; Rouse, M. *Appl. Catal., B* **1998**, *17*, 25. (b) Heller, A. *Acc. Chem. Res.* **1995**, *28*, 503. (c) Herrmann, J.-M.; Tahiri, H.; Ait-ichou, Y. A.; Lassaletta, G.; González-Elipe, A. R.; Fernández, A. *Appl. Catal., B* **1997**, *13*, 219.

(7) (a) Mardare, D.; Tascu, M.; Delibas, M.; Rusu, G. I. *Appl. Surf. Sci.* **2000**, *156*, 200. (b) Suzuki, S. *Thin Solid Films* **1999**, *351*, 194.

(8) Lee, W. G.; Woo, S. I.; Kim, J. C.; Choi, S. H.; Oh, K. H. *Thin Solid Films* **1994**, *237*, 105.

(9) Kim, E. K.; Son, M. H.; Min, S. K.; Han, Y. K.; Wang, C. H.; Yom, S. S. *J. Appl. Phys.* **1996**, *79*, 4459.

(10) Halary, E.; Benvenuti, G.; Wagner, F.; Hoffmann, P. *Appl. Surf. Sci.* **2000**, *154–155*, 146.

(11) Escobar-Alarcón, L.; Haro-Poniatowski, E.; Camacho-López, M. A.; Fernández-Guasti, M.; Jimenez-Jarquín, J.; Sánchez-Pineda, A. *Appl. Surf. Sci.* **1999**, *137*, 38.

(12) Bhattacharyya, D.; Sahoo, N. K.; Thakur, S.; Das, N. C. *Thin Solid Films* **2000**, *360*, 96.

(13) Sammelselg, V.; Rosental, A.; Tarre, A.; Niinistö, L.; Heiskanen, K.; Ilmonen, K.; Johansson, L.-S.; Uustare, T. *Appl. Surf. Sci.* **1998**, *134*, 78.

(14) (a) Jämting, Å.K.; Bell, J. M.; Swain, M. V.; Wielunski, L. S.; Clissold, R. *Thin Solid Films* **1998**, *332*, 189. (b) Lin, H.; Kozuka, H.; Yoko, T. *Thin Solid Films* **1998**, *315*, 111. (c) Nishide, T.; Mizukami, F. *Thin Solid Films* **1999**, *353*, 67.

(15) Natarajan, C.; Nogami, G. *J. Electrochem. Soc.* **1996**, *143*, 1547.

(16) Oswald, M.; Hessel, V.; Riedel, R. *Thin Solid Films* **1999**, *339*, 284.

films being their inherited properties from the native colloids such as photochromic,¹⁹ photoelectrochemical,²⁰ and photocatalytic properties.²¹ However, in these methods an annealing posttreatment, usually at 450 °C, is necessary to remove the organics used in the preparation of the colloidal suspension or paste. The thermal treatment also favors the adhesion of the titania to the substrate and increases the electric conductivity (the sheet resistance decreases) because of a better cohesion between particles.

It is evident the interest of low-temperature methods for fabrication of crystalline thin films of advanced materials²² such as semiconductors, ceramics, or their composites and/or hybrids, not only from the point of view of energy saving, as annealing posttreatment is avoided, but also as they allow the use of low thermally resistant materials such as plastics, wood, or paper as substrates. Furthermore, to make the whole chemical approach environmental friendly, the use of aqueous solutions instead of organic solvents is desired.

Recently, our group has accomplished the deposition of anatase TiO₂ films with relative ease and at low-temperature using a new soft-solution processing method in which crystallization is enhanced by microwave heating.²³ In this paper we show a new method in which colloidal anatase is deposited on different substrates by a drain-coating process employing a colloidal aqueous solution at 333 K.

Experimental Section

Reagents. Chemicals were of reagent grade and were used without further purification: tetraisopropyl orthotitanate (TIP; Fluka); tetrabutylammonium hydroxide ((TBA)OH; 40% in water, Fluka); absolute ethanol (EtOH; Panreac); salicylic acid (Merck). The water employed in all preparations was purified by a Milli-Q system (Millipore).

Preparation of Aqueous Colloidal Solution. Anatase nanocrystals were prepared by the controlled hydrolysis of TIP as described previously,²⁴ with minor modifications. TIP (5 mL) was dissolved in absolute EtOH (30 mL), and the solution was added to a solution of 0.6 mL of (TBA)OH (40% in water) in 30 mL of absolute EtOH. Both solutions were preserved from atmosphere moisture before their mixture. Afterward, 185 mL of water was added. The obtained transparent solution, with a 19:1 Ti:TBA molar ratio, was heated to evaporate ethanol and 2-propanol (the TIP hydrolysis byproduct) until the volume of the solution was reduced to ca. 100 mL. This solution was heated to reflux for 2 h by means of a microwave furnace (Prolabo Maxidigest MX350) working at 60 W. After this

treatment, a transparent slightly blue-colored aqueous colloidal solution was recovered. Unless otherwise stated, a 5-fold diluted solution was used. To gain further knowledge, non MW-treated solutions, although not used in deposition experiments, were also studied. In both cases, solid samples for powder XRD characterization were obtained from aliquots dried at 333 K.

Substrates. Anatase nanoparticles were deposited on glass, F-doped SnO₂-covered glass (referred as TCO from now on) and Si(100) wafers. Glass slides were immersed both in boiling sulfuric acid and boiling Milli-Q water for 30 min, and afterward they were ultrasonically cleaned in acetone and absolute EtOH for 5 min. Finally, they were rinsed with water. TCO substrates with sheet resistance 15 Ω/□ (Flabeg, Pilkington Group) were ultrasonically cleaned in acetone and absolute EtOH for 5 min and rinsed with water. Si substrates were ultrasonicated in absolute EtOH and in acetone for 5 min. Afterward, Si substrates were rinsed with water and cleaned with diluted HF to dissolve silicon oxide. Finally, they were thoroughly rinsed with water.

Au: In the above paragraph, 4th sentence from the end, please check units for sheet resistance.

Deposition Method. For film preparation, the drain-coating method in which the substrate remains stationary while the solution is drained from the vessel was employed. Substrates were immersed for 5 min into 100 mL of the colloidal solution, which was maintained at 333 K in a thermostated vessel. Afterward, the solution level was lowered at a rate of 23 mm/min by means of a peristaltic pump connected to an open end in the bottom of the vessel. Upon removal from the solution, the substrate was carefully rinsed with water and dried under N₂ flow. Films so obtained were well-adhered. Adhesion was qualitatively evaluated by submerging the film in a beaker containing water and submitting to ultrasonic vibrations (Selecta, 50 W) for 5 min. No modification of the optical interference fringes was observed. TiO₂ layers on substrates could be thickened by means of consecutive drain-coating processes. In these experiments, substrates were immersed only for 1 min after the first draining process and were only rinsed with water and dried with N₂ at the end of the whole deposition process.

Characterization Techniques. Characterization of the dried colloid powder by X-ray diffraction (XRD) was carried out with a Rigaku Rotaflex RU-200B with Cu Kα radiation, operated at 50 kV and 80 mA over the range 10 < 2θ < 60°. Fluorescence spectra of the TiO₂ colloidal solutions were recorded on a Perkin-Elmer LS 50 luminescence spectrometer at room temperature; an excitation wavelength of 252 nm was employed. For TEM studies, a drop of 10-fold-diluted colloidal solution was directly deposited on carbon-coated copper grids. Observations were made with a Philips CM30 microscope working at 300 kV. Fourier transform infrared spectra (FTIR) of TiO₂ nanocrystallites onto Si substrates were recorded in a Perkin-Elmer System 2000 FT-IR. Optical absorption spectra (UV-vis) of colloidal solutions and films on glass and TCO substrates were recorded in the absorption mode using a Hewlett-Packard diode array spectrometer (model 8453) at a resolution of 1 nm. Grazing-angle X-ray diffraction patterns of the deposited films were recorded on a Siemens D-3400 apparatus operated at 40 kV and 30 mA. The diffraction data were recorded at different X-ray incidence angles over the range 15 < 2θ < 60°.

Photocatalysis. The photoactivity of TiO₂ films on glass slides was evaluated by the degradation of salicylic acid under UV illumination. Experiments were conducted in a thermostated cylindrical Pyrex cell of 130 cm³ capacity in which temperature was kept at 298 K. A 125 W Philips HPK medium-pressure mercury vapor lamp was used as light source. A 6.25 × 10⁻⁵ mol L⁻¹ salicylic acid solution (100 mL) was employed. Films for photocatalytic experiments were prepared by 25 consecutive drain-coating processes, resulting approximately in 2 × 10⁻² mg TiO₂ cm⁻². The solution inside the cell was stirred, and air was bubbled into it during the whole experiment. Absorbance of initial and irradiated samples was determined with a Philips PU 8620 UV/vis/NIR spectro-

(17) (a) Xiao, Z.; Gu, J.; Huang, D.; Lu, Z.; Wei, Y. *Appl. Surf. Sci.* **1998**, *125*, 85. (b) Shin, H.; Collins, R. J.; de Guire, M. R.; Heuer, A. H.; Sukenik, C. N. *J. Mater. Res.* **1995**, *10*, 692. (c) Kovtyukhova, N.; Ollivier, P. J.; Chizhik, S.; Dubravina, A.; Buzaneva, E.; Gorchinskiy, A.; Marchenko, A.; Smirnova, N. *Thin Solid Films* **1999**, *337*, 166.

(18) Kamat, P. V. *Chemtech* **1995**, June, 22.

(19) Torimoto, R.; Fox, R. J., III; Fox, M. A. *J. Electrochem. Soc.* **1996**, *143*, 3712.

(20) (a) Hagfeldt, A.; Björkstén, U.; Lindquist, S.-E. *Sol. Energy Mater. Sol. Cells* **1992**, *27*, 293. (b) Kozuka, H.; Takahashi, Y.; Zhao, G.; Yoko, T. *Thin Solid Films* **2000**, *358*, 172.

(21) Zeltner, W. A.; Hill, Jr. C. G.; Anderson, M. A. *Chem. Technol.* **1994**, 21.

(22) Yoshimura, M. *J. Mater. Res.* **1998**, *13*, 796.

(23) (a) Vigil, E.; Saadoun, L.; Ayllón, J. A.; Domènech, X.; Zumeta, I.; Rodríguez-Clemente, R. *Thin Solid Films* **2000**, *365*, 12. (b) Vigil, E.; Saadoun, L.; Rodríguez-Clemente, R.; Ayllón, J. A.; Domènech, X. *J. Mater. Sci. Lett.* **1999**, *18*, 1067. (c) Vigil, E.; Ayllón, J.; Peiró, A. M.; Rodríguez-Clemente, R.; Domènech, X.; Peral, J. *Langmuir* **2001**, *17*, 891.

(24) Saadoun, L.; Ayllón, J. A.; Jiménez-Becerril, J.; Peral, J.; Domènech, X.; Rodríguez-Clemente, R. *Mater. Res. Bull.* **2000**, *35*, 193.

photometer at a wavelength of 296 nm, using a quartz cuvette of 4 cm of optical path length.

Results and Discussion

Anatase TiO₂ Colloid Characterization. Preliminary work has shown that (TBA)OH can be used as hydrolysis control agent for the production of anatase TiO₂ from titanium alcoxides.²⁴ When an alcoholic solution of TIP is mixed with a mostly alcoholic (TBA)-OH solution (obtained from the dilution of a concentrated aqueous solution of (TBA)OH in a relatively large amount of absolute ethanol), the precipitation of titanium hydroxide does not take place even when a great amount of water is added afterward, and transparent colloidal solutions are obtained. Other ways of using a tetraalkylammonium hydroxide ((TAA)OH) for the synthesis of TiO₂ are described in the literature.^{25–27} In these works a titanium alkoxide precursor is first hydrolyzed by water yielding an amorphous precipitate of titanium hydroxide, and a (TAA)OH, often tetramethylammonium hydroxide, is added afterward to control further peptization and crystallization, which are achieved by relatively severe processes such as autoclaving^{26,27} or prolonged reflux treatment.^{25, 27}

In our case, a faster treatment, such as microwave irradiation for 2 h, is used to enhance the crystallization of the titania precursor. Previous to MW treatment, most alcohols from the mixture are eliminated by evaporation. This step allows one to raise by some degrees Celsius the refluxing temperature of the solution during microwave treatment and, particularly, gives an aqueous solution that can be more easily manipulated, as no organic vapors are produced. In addition, it has been reported that water favors crystallinity of titania, while alcohol presents the contrary effect.²⁸

In this work colloidal TiO₂ was prepared by following our previously described method²⁴ but with a 19:1 Ti:TBA molar ratio instead of the 10:1 ratio reported. This change was made to reduce the content of organics in the colloidal solution. Although titania growth control is necessary, the presence of organics in the final product is very undesirable. However lower concentrations of (TBA)OH did not show a full stabilizing effect.

To characterize the crystal structure of TiO₂ nanoparticles in the colloidal solution, 30 mL of colloid was evaporated at 333 K, yielding a bright water-dispersible yellow solid which was examined by XRD. Figure 1a shows the XRD pattern of this solid, in which broad peaks are observed at values of 2θ equal to 25.6, 38.1, 48.2, and 54.7° that correspond to the anatase structure. An small broad signal at 31° (arrow) is ascribed to TiO₂ brookite traces. No differences were observed between XRD patterns of samples evaporated immediately after colloid preparation or 20 days later. Indeed, colloidal solutions were kept at room temperature in closed

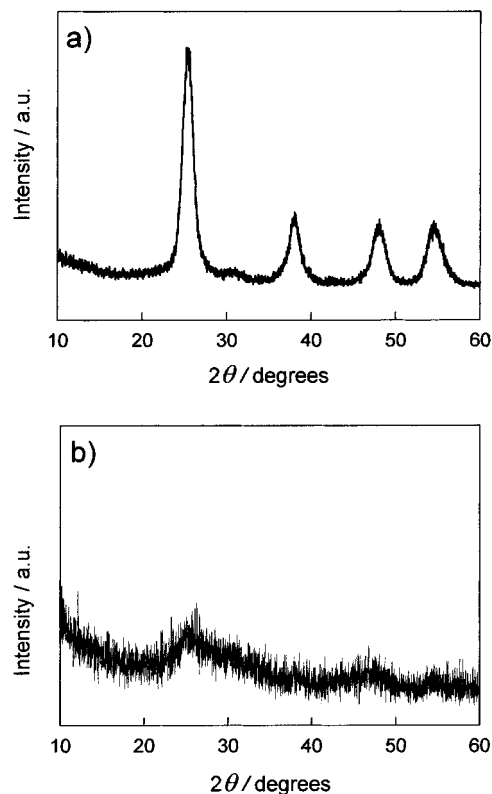


Figure 1. X-ray diffraction patterns of TiO₂ crystallites obtained after evaporating the colloidal solution at 333 K: (a) after and (b) before MW treatment.

vessels for several months without any change being observed. The pH of these solutions is close to 10.5, a value certainly higher than PZC (point zero charge) values reported for TiO₂.²⁹ At this pH, nanoparticles are negatively charged. Indeed, it is well-known that a strong base as (TBA)OH favors the formation of Ti–O[−] groups on the TiO₂ surface.^{27,30} TBA cations supply the counteracting positive charge. To assess the effect of MW, further experiments with non-MW-treated solutions were performed. Figure 1b shows the XRD pattern of the solid recovered after evaporation at 333 K of non-MW-treated colloid. Only a very broad signal centered at ca. 24–28° is observed. This fact suggest that TiO₂ crystallites have a very small size, which must be about 1 nm.³¹

Morphology and size of colloidal nanoparticles after MW treatment were examined by transmission electron microscopy (TEM). Figure 2 shows elongated box-shaped particles with a particle size distribution of about 7–11 nm length and 3–6 nm width.

Figure 3 shows the UV–vis spectra of the colloidal solution before and after MW treatment. There is no optical absorption at $\lambda > 370$ nm, suggesting that the slight blue color may result from the luminescence of the colloids;³² some contribution due to the Tyndall effect cannot be discarded. These spectra were processed in order to obtain the energy band gap, E_g , from the

(25) Moritz, T.; Reiss, J.; Diesner, K.; Chemseddine, A. *J. Phys. Chem. B* **1997**, *101*, 8052.

(26) Burnside, S. D.; Shklover, V.; Barbé, C.; Comte, P.; Arendse, F.; Brooks, K.; Grätzel, M. *Chem. Mater.* **1998**, *10*, 2419.

(27) Chemseddine, A.; Moritz, T. *Eur. J. Inorg. Chem.* **1999**, 235.

(28) Yin, S.; Inoue, Y.; Uchida, S.; Fujishiro, Y.; Sato, T. *J. Mater. Res.* **1998**, *13*, 844.

(29) Kormann, C.; Bahnemann, D. W.; Hoffmann, M. R. *J. Phys. Chem.* **1988**, *92*, 5196.

(30) Livage, J.; Henry, M.; Sanchez, C. *Prog. Solid State Chem.* **1998**, *18*, 259.

(31) Monticone, S.; Tufeu, R.; Kanaev, A. V.; Scolan, E.; Sanchez, C. *Appl. Surf. Sci.* **2000**, *162–163*, 565.

(32) Liu, Y.; Claus, R. O. *J. Am. Chem. Soc.* **1997**, *119*, 5273.

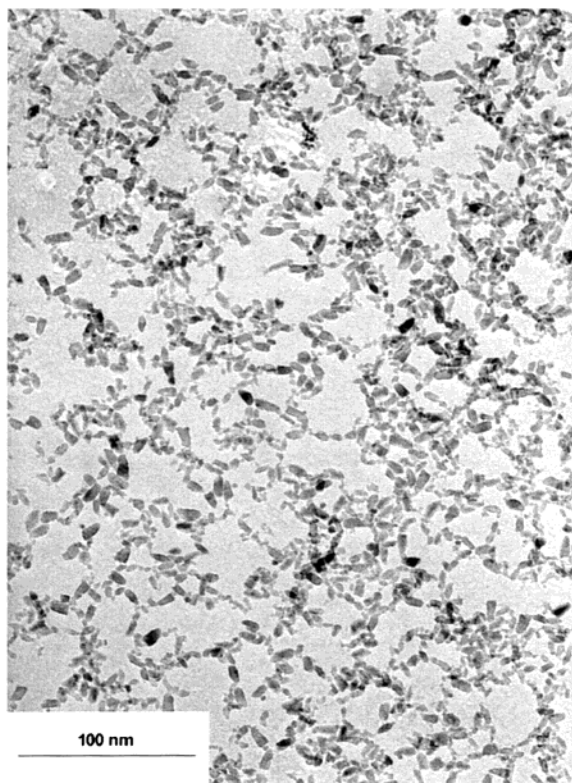


Figure 2. TEM images corresponding to anatase nanocrystallites after MW treatment.

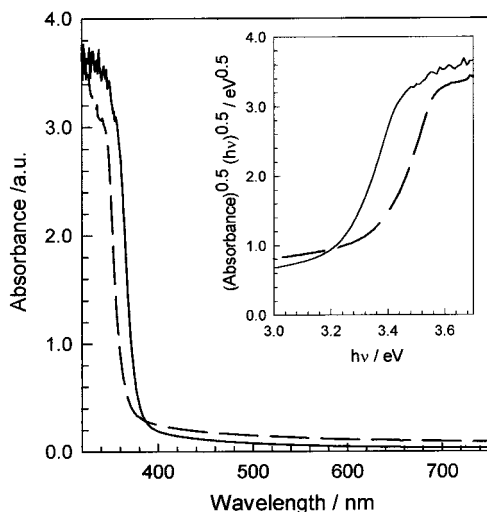


Figure 3. UV-vis spectra of anatase colloid solution: (dashed line) before and (solid line) after MW treatment. Insert: Variation of $(\text{absorbance})^{0.5}(h\nu)^{0.5}$ with excitation energy ($h\nu$) for the anatase colloid to identify indirect transitions.

expression corresponding to indirect gap semiconductors (insert in Figure 3):

$$\alpha(h\nu)h\nu \propto (h\nu - E_g)^2$$

Here α is the absorption coefficient (cm^{-1}) and $h\nu$ (eV) is the energy of excitation. From these plots, a value of E_g of 3.28 eV is obtained for the colloid after MW treatment, which is ascribed to bulk anatase (3.18 eV),³³ and a value of 3.41 eV for colloid before MW treatment.

(33) Serpone, N.; Lawless, D.; Khairutdinou, R. *J. Phys. Chem.* **1995**, *99*, 16646

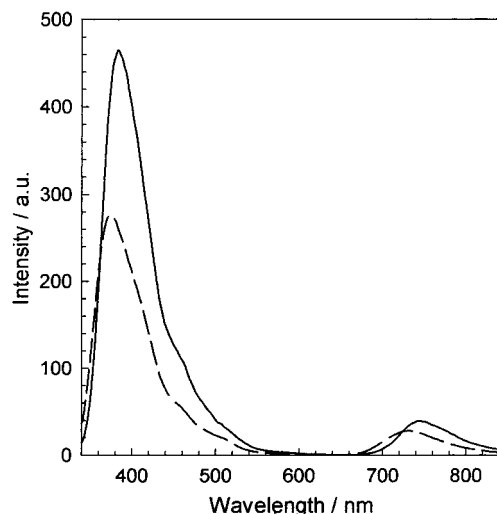


Figure 4. Fluorescence spectra of the anatase colloid at two stages of the preparation: (dashed line) before and (solid line) after MW treatment. In the later case the intensity of spectra has been 10-fold divided to facilitate comparisons. Experimental conditions: room temperature; excitation wavelength = 252 nm.

In this latter case, an increase of the band gap energy, and therefore a blue shift in the absorption edge, is in accordance with the effects of quantization with decreasing particle size that have been accounted in several studies for very small TiO_2 colloid particles ($d < 4 \text{ nm}$)³⁴ and even for larger particles ($d < 10.8 \text{ nm}$).³⁵

To further characterize the TiO_2 colloidal solution, fluorescence spectra were recorded at various stages of the preparation. Figure 4 shows the fluorescence spectra of the colloidal solution before and after MW irradiation. Bands with a broad spectral width were observed in both cases. For MW-treated colloids (solid line), a sharp increase after 340 nm is observed, reaching a maximum at 384 nm. As in refs 32 and 36, most of the fluorescence of the colloidal TiO_2 takes place in the blue portion of the visible spectrum and diminishes toward the green portion of the spectrum. The emission maximum corresponds to the band gap (3.23 eV) of the bulk semiconductor. Single-crystal semiconductors show a sharp emission maximum corresponding to the band gap. On the contrary, the spectrum has a half-width of ca. 61 nm and tails up to 562 nm, this broad emission being typical of semiconductor-particle suspensions in water. Fluorescence between 600 and 900 nm is associated with transitions of electrons from the conduction band edge to holes trapped at an interstitial Ti^{3+} site.³⁷ Fluorescence spectrum recorded before MW irradiation (dashed line) presents a similar shape to that of the irradiated colloid but its intensity is less than 1/10. In addition, a blue shift displacement of approximately 10 nm in the whole spectrum is observed. These results suggest that incipient tiny nucleus of crystalline TiO_2

(34) (a) Choi, V.; Termin, A.; Hoffmann, M. R. *J. Phys. Chem.* **1994**, *98*, 13669. (b) Bahnmann, D. W. *Isr. J. Chem.* **1992**, *33*, 115. (c) Joselevich, E.; Willner, I. *J. Phys. Chem.* **1994**, *98*, 7628. (d) Anpo, M.; Shima, T.; Kodama, S.; Kubokawa, Y. *J. Phys. Chem.* **1987**, *91*, 4305.

(35) Sun, F.; Wu, M.; Li, W.; Li, X.; Gu, W.; Wang, F. *Cuihua Xuebao* **1998**, *19*, 3229.

(36) Chandrasekaran, K.; Thomas, J. K. *J. Chem. Soc., Faraday Trans.* **1984**, *80*, 1163.

(37) Samtsov, M. P. *J. Electroanal. Chem.* **1992**, *340*, 73.

must be present, although not being detectable by XRD (amorphous TiO₂ colloids do not show fluorescence).³⁶

As a conclusion, particles exhibiting quantum-sized effects (blue-shift in UV–vis and fluorescence spectra) are obtained before MW treatment of the colloidal solution. To enhance the growth of these particles, and hence to obtain particles with bulk properties, which require less energy to promote an electron from the valence band to the conduction band, a MW irradiation treatment is performed, which yields the desired stable colloidal solution.

Anatase TiO₂ Thin-Film Characterization. TiO₂ nanoparticles were deposited onto different substrates, such as glass, silicon, and TCO, by a drain-coating method performed at 333 K. To assess if layer thickness was dependent upon the time of immersion of substrates in the colloidal solution previous to the draining process, several experiments were performed at different times of immersion ranging from 5 to 60 min, before draining at the same rate. No significant differences in UV–vis spectra of these layers were observed. This fact suggests that deposition of TiO₂ onto the substrates does not take place in the solution bulk. However, it was observed that the draining rate clearly affects the homogeneity of the films. Hence, it is inferred that deposition takes place when the solution drains near the interface between the aqueous solution, the glass substrate, and the air, i.e., at the meniscus. Actually, homogeneous films were only obtained when a uniform movement of such interface was achieved. It has been observed that deposited films do not disperse in water, while the solid sample obtained after evaporation of the colloidal solution on the substrate could be redispersed in water, both processes being performed at the same temperature. The redispersion of the solid obtained after simple evaporation could be explained considering that the junction among anatase nanocrystals is hindered by their surface negative charge due to adsorbed hydroxyl anions and by the presence of TBA cations. Further, the films obtained by the drain-coating process are well-adhered, as denoted by their resistance to ultrasonic vibrations. These facts account for some other mechanism taking place in the meniscus rather than simple evaporation of the colloidal solution onto the substrate.

A first hypothesis for the mechanism of film formation was that neutral TiO₂ nanocrystals were deposited in the meniscus. This fact would imply that no TBA cations are present in films, as nanoparticles lose their excess hydroxyl groups, which remain in solution together with their corresponding TBA counteracting cations (see detailed explanation below). To confirm the lack of TBA cations in films, FT-IR spectra were analyzed for films deposited onto Si(100). On one hand, a drop of diluted aqueous colloidal solution was evaporated onto Si(100); the FTIR spectrum (Figure 5a) revealed several peaks assignable to TBA cations (i.e. 2967, 1485, 1369 cm⁻¹), as well as a broad band corresponding to bulk TiO₂ skeletal frequency region (below 730 cm⁻¹).³⁸ The presence of water was also manifested. On the other hand,

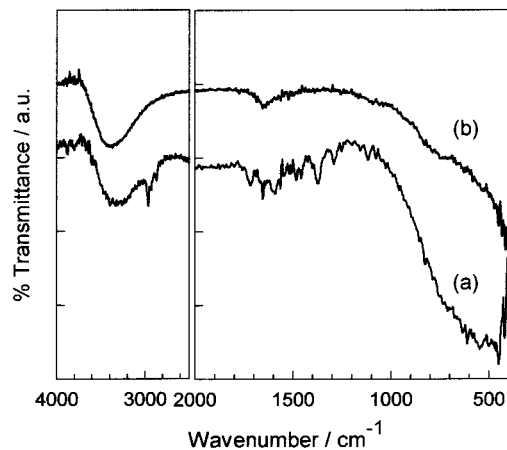
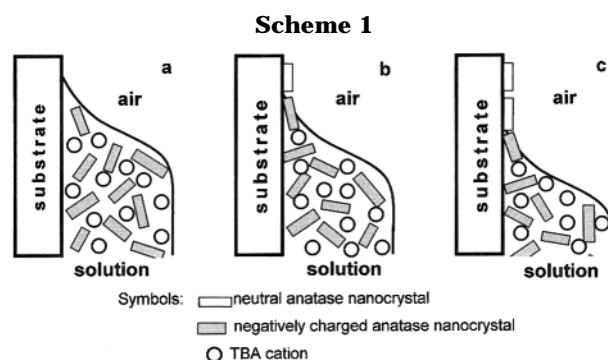


Figure 5. FTIR spectra of anatase colloidal solution deposited on Si substrates: (a) a drop of colloidal solution deposited and then evaporated; (b) deposition performed by the drain-coating method.



a 6-fold drain-coated Si(100) sample was studied. The FT-IR spectrum of this sample shows only tiny peaks corresponding to organic compounds (Figure 5b), while the presence of TiO₂ is clearly denoted by the absorbance in the region below 800 cm⁻¹.³⁸ Therefore, it was concluded that TiO₂ nanocrystallites deposited by the drain-coating method are mainly free of TBA cations. To explain such an experimental finding, a tentative simplified mechanism is proposed (see Scheme 1), in which liquid–solid and liquid–air interfaces are represented. Scheme 1a shows the colloidal solution, consisting of negatively charged anatase nanoparticles stabilized by tetrabutylammonium cations (TBA⁺), in contact with the substrate surface. Scheme 1b shows the situation once the solution level has been lowered and, hence, the deposition process has started. Some TiO₂ crystallites have been deposited onto the substrate surface. We suggest that when anatase nanocrystals at the meniscus anchor to the substrate, they become neutral; their excess of negative charges is lost as hydroxyl anions. Then, these OH⁻ anions and, consequently, TBA⁺ counterions are drawn to the solution. Classic models concerning surface tension of electrolyte solutions state that charged inorganic species tend to avoid the air–water interface and concentrate in the solution bulk.³⁹ However, recent ab initio calculation on NaCl solutions in water show that ions do not uniformly distribute in the air–water interface; chloride anions actually accumulate near the water surface.⁴⁰

(38) (a) Harizanov, O.; Harizanova, A. *Sol. Energy Mater. Sol. Cells* **2000**, *63*, 185. (b) Kaliwot, N.; Zhang, J.-Y.; Boyd, I. W. *Surf. Coat. Technol.* **2000**, *125*, 424. (c) González, R. J. Ph.D. Thesis, Virginia Polytechnic Institute, Blacksburg, VA, 1996.

(39) Levine, I. N. *Physical Chemistry*, 4th ed.; McGraw-Hill: New York, 1996; Vol. 1, p 391.

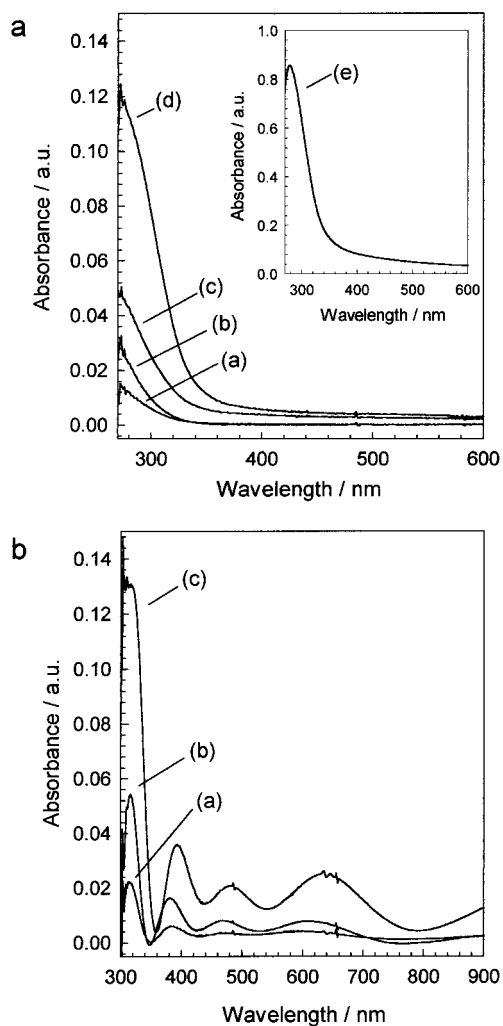


Figure 6. (a) UV-vis spectra of TiO₂ layer on glass substrates after (a) 1, (b) 10, (c) 15, (d) 20, and (e) 25 (insert) drain-coating processes with anatase colloid. (b) UV-vis spectra of TiO₂ layer on TCO substrates after (a) 1, (b) 5, and (c) 15 drain-coating processes with anatase colloid.

The good adherence of the film to the substrate suggests that strong joining forces act between the substrate and the deposited crystallites. Strong covalent oxo bridges ($>X-O-Ti<$; $X = Si, Sn$) could account for the good adherence reported.

The thickness of the TiO₂ layer as a function of the number of repeated deposition processes was studied. The thinnest layers were transparent and colorless, while in the thickest ones interference colors were observed. Figure 6a shows the UV-vis absorption spectra of films deposited on glass after 1, 10, 15, 20, and 25 drain-coating processes, respectively. This figure shows that absorption, and consequently the thickness of the layer, are enhanced when the number of deposition processes increases.

The amount of TiO₂ deposited in each process is small, as estimated by gravimetry: a 25-fold drain-coated glass substrate contains approximately 2×10^{-2} mg of TiO₂ cm⁻², i.e., a layer thickness of 54 nm, considering the whole layer as being compact. In fact, this is a minimum value as a porous layer rather than a compact one is obtained by the actual mechanism of deposition. This

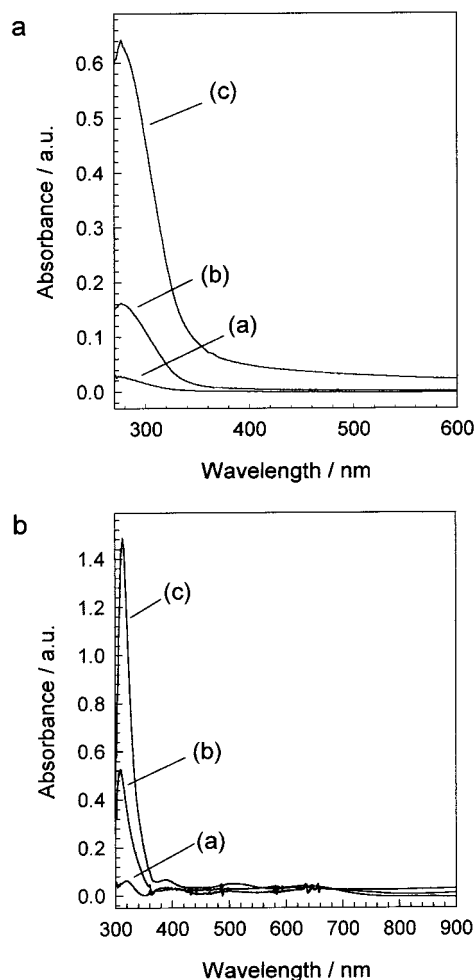


Figure 7. (a) UV-vis spectra of TiO₂ layer on glass substrates after (a) 1, (b) 10, and (c) 15 drain-coating processes with concentrated anatase colloid solution. (b) UV-vis spectra of TiO₂ layer on TCO substrate after (a) 1, (b) 10, and (c) 15 drain-coating processes with concentrated anatase colloid solution.

means that, at least, about 2 nm of layer is deposited in each coating, yielding a submonolayer coverage (as confirmed by AFM). On subsequent coating processes, the previously deposited anatase crystallites act as substrate. In this case the anchorage is favored as homojunctions are more easily formed than heterojunctions. This fact explains the faster growth in thickness with an increasing the number of drain-coating processes (see Figure 6a).

From UV-vis spectra, the corresponding E_g values could be determined. Indeed, calculated values for the thinnest films were higher than expected due to experimental limitations related to the employed technique. However, for films produced after at least 15 drain-coating processes, band gap values correspond to bulk TiO₂ anatase. Figure 6b shows the UV-vis absorption spectra of films deposited on TCO after 1, 5, and 15 drain-coating processes. Absorption maxima increments with the number of drain-coating processes were more pronounced for layers deposited onto TCO than onto glass.

Figure 7 shows UV-vis absorption spectra of films deposited after 1, 10, and 15 drain-coating processes with concentrated colloid solution onto glass (Figure 7a) and onto TCO substrate (Figure 7b). Thicker layers were

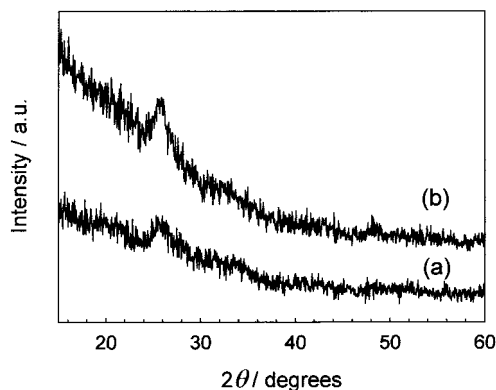


Figure 8. X-ray diffraction pattern of TiO₂ layer on glass after 1 and 10 drain-coating processes with anatase colloid (bottom and top, respectively).

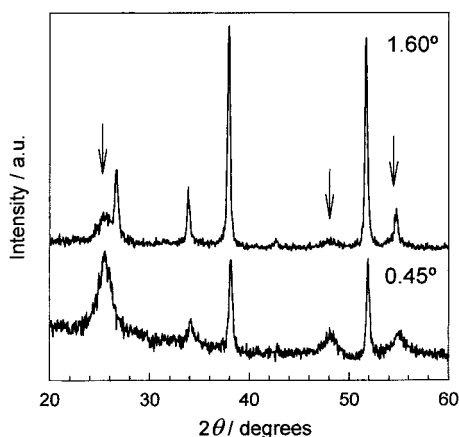


Figure 9. Grazing-angle XRD pattern of TiO₂ layer on TCO after 15 drain-coating processes with anatase colloid at two different grazing incidence angles: 0.45 and 1.60° (top and bottom, respectively). For an angle of incidence of 0.45°, TiO₂ anatase peaks are observed (marked with an arrow), as well as peaks corresponding to the substrate. For 1.60°, the depth of X-ray penetration into the film is higher and peaks corresponding to the substrate are more intense.

obtained from concentrated colloidal solution compared to diluted ones for the same number of deposition processes. Moreover, again a more pronounced absorbance increase for layers deposited onto TCO compared to glass is observed. The fact that TiO₂ nanoparticles are more easily deposited onto TCO than onto glass can be explained by considering that the crystalline nature of the TCO surface induces a faster growth of the TiO₂ layer, compared with the amorphous surface of glass.

XRD experiments were performed to further confirm the crystallinity of the deposited materials, which had already been inferred by the optical properties of the films. Figure 8 shows the X-ray diffraction pattern of TiO₂ layers on glass after 1 and 10 drain-coating processes with anatase colloid. Broad peaks were observed for the thickest layers which were assigned to anatase structure. It was not possible to characterize the thinnest layers by XRD. For films formed onto TCO, anatase structure was also found (see Figure 9).

Photocatalysis with the TiO₂ Thin Films. The photocatalytic activity of the films toward the degradation of salicylic acid in aqueous solutions was investigated. Figure 10 shows the percentage of salicylic acid

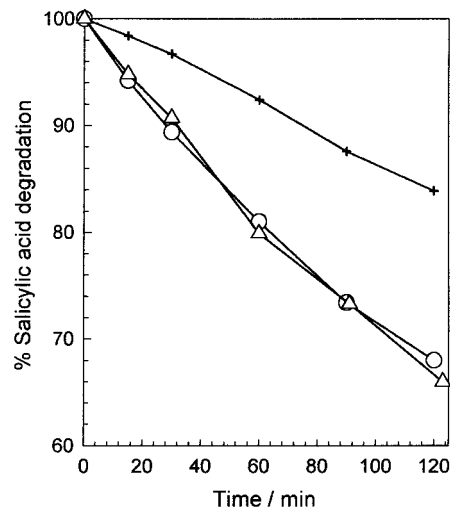


Figure 10. Percentage of salicylic acid removed with irradiation time for aqueous suspensions (6.25×10^{-5} mol L⁻¹; 100 cm³) in the presence of nanocrystalline anatase films prepared by 25 consecutive drain-coating processes (ca. 2×10^{-2} mg TiO₂ cm⁻²). Experimental conditions: UV irradiation; 298 K; stirred; air was bubbled. Key: (+) clean substrate; (O) films without thermal treatment; (Δ) films with thermal treatment (675 K, 2 h).

degraded as a function of irradiation time for different treated TiO₂ films. As previously reported, titania powders obtained from a similar aqueous colloidal solution with a Ti:TBA 10:1 molar ratio presented photocatalytic activity in the gas-phase oxidation of formaldehyde after calcination to eliminate TBA cations.²⁴ In the present study, however, no annealing posttreatment was necessary to eliminate TBA cations, as they were not present in deposited TiO₂ films. For photocatalytic essays, 25-fold drain-coated glass substrates were used. Figure 10 shows the results of photocatalytic activity of two TiO₂ films, (i) an as-deposited film not annealed and (ii) a heat-treated sample at 675 K for 2 h. As can be seen, no difference in the degradation rate is found between both samples; this fact implies that no annealing treatment is necessary in the present case to induce crystallinity in samples in order to improve photocatalytic activity, as is the general case.⁴¹ It must be signaled that after these experiments no loss in the photocatalytic activity of films was detected.

In conclusion, it has been shown that nanocrystalline TiO₂ anatase stabilized by (TBA)OH can be deposited onto different substrates with a method performed at low temperature, yielding photoactive material for the degradation of a liquid-phase contaminant.

Acknowledgment. This work was financed by the AMB-12R-CO3-01 CICYT project of the Spanish National Plan of Research. The authors thank Flabeg (Pilkington group) for kindly supplying TCO substrates and Dra. Agustina García (Institut de Biologia Fonamental-UAB) for providing luminescence equipment.

CM0012419

(41) Pozzo, R. L.; Baltanás, M. A.; Cassano, A. E. *Catal. Today* **1997**, *39*, 219.

